Full Coherent Frequency Conversion between Two Propagating Microwave Modes

Baleegh Abdo,[*] Katrina Sliwa, Flavius Schackert, Nicolas Bergeal,[†] Michael Hatridge, Luigi Frunzio,
A. Douglas Stone, and Michel Devoret[‡]

Department of Applied Physics, Yale University, New Haven, Connecticut 06520, USA
(Received 10 December 2012; published 26 April 2013)

We demonstrate full frequency conversion in the microwave domain using a Josephson three-wave mixing device pumped at the difference between the frequencies of its fundamental eigenmodes. By measuring the signal output as a function of the intensity and phase of the three input signal, idler, and pump tones, we show that the device functions as a controllable three-wave beam splitter or combiner for propagating microwave modes at the single-photon level, in accordance with theory. Losses at the full conversion point are found to be less than 10^{-2}. Potential applications of the device include quantum information transduction and realization of an ultrasensitive interferometer with controllable feedback.

A quantum information transducer capable of converting the frequency of a quantum signal without introducing noise is one of the desirable modules in quantum communication [1,2]. With such a device, one could teleport quantum superpositions of ground and excited states of qubits from one system to another with a different transition frequency, without loss of coherence. If a quantum signal can be routed through different frequency channels, optimization of quantum calculation and communication can be advantageously separated.

The simplest scheme for performing frequency conversion is pumping a dispersive medium with nonlinearity χ_2 at precisely the frequency difference between the input and output frequencies [3–10]. Such nonlinear process known as parametric frequency conversion holds the promise of converting the frequency in a unitary, therefore noiseless, manner, namely, without adding loss or dephasing to the processed signal [11]. In the optical domain, although the intrinsic conversion process can be unitary [12–15], technical issues such as filtering the converted signal from noise photons generated via Raman processes and residual pump photons can limit the practical end-to-end conversion efficiency. In the microwave domain, nonlinear elements used in mixers such as Schottky diodes are by contrast intrinsically dissipative and inevitably lead to unacceptable conversion losses. This raises the question as to whether a unitary full conversion of an input signal can be realized practically.

Here, we show that such noiseless full conversion is possible in the microwave domain by operating a dissipationless three-wave mixing element known as the Josephson parametric converter (JPC) [16–18], in a regime of conversion without photon gain. The JPC performs frequency conversion from 8 to 15 GHz with losses below 0.05 dB at full conversion, as opposed to a typical loss of 6 dB in microwave mixers. We reveal the unitary nature of the JPC conversion by utilizing wave interference between the three incommensurate frequencies intervening in the

device. The coherence of the conversion process is thus verified without the challenging calibration of the transmission between different input and output lines of disparate frequencies.

To introduce the requirements obeyed by the properties of unitary frequency conversion, we compare in Fig. 1 a
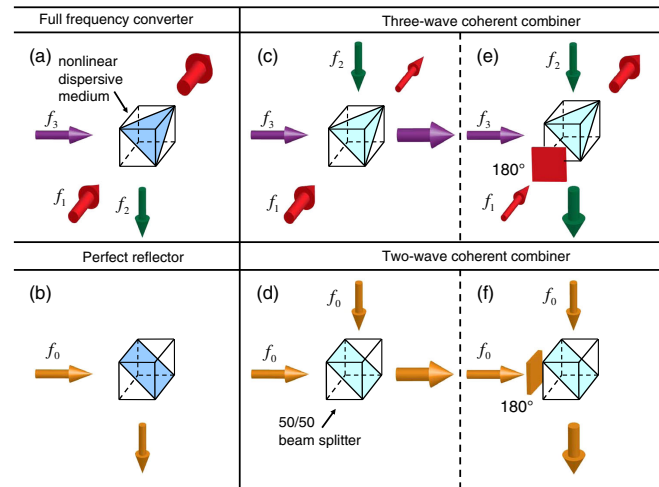

FIG. 1 (color online). In a three-wave coherent converter, the scattered beams have different frequencies which we indicate using different colors: violet, green, and red. Panel (a) depicts a nonlinear dispersive medium operated as a full frequency converter for the incident violet and green beams. Panel (b) depicts a splitter modified into a perfect mirror which constitutes the two-wave analogue of the full frequency converter. Panels (c) and (e) introduce the relationship between frequency conversion and three-wave interference. By operating the device shown in panel (a) as a three-wave 50/50 beam combiner, one can coherently interfere two equal photon flux beams (green and violet) with disparate frequencies via frequency conversion through the third beam (red). Conversely, in a two-wave coherent beam splitter or combiner, complete interference can take place [panels (d) and (f)] when two equal intensity beams with the same frequency are incident at the beam splitter.

three-wave coherent converter and a two-wave coherent
beam splitter. Figure 1(a) depicts the desired case of unitary
full frequency conversion of an incident propagating beam,
i.e., a violet (high frequency) to a green (low frequency)
beam, obtained by pumping with adequate strength a dis-
persive χ_2 medium with a red beam whose frequency is
precisely the frequency difference between the violet and
green. In Fig. 1(b) we depict the two-wave analogue of such
a device; that is, the total reflector whose input and output
beams have the same frequency and magnitude but propa-
gate in different directions. Figures 1(c) and 1(e) depict the
same three-wave coherent converter shown in Fig. 1(a),
now operated at the 50/50 beam-splitting point. At this
working point, the device transmits half of the power of the
input beams (green and violet) and converts the frequency
of the other half, using the third red (pump) beam. Hence,
Figs. 1(c) and 1(e) describe destructive interference (DI)
scenarios for the two equal photon flux input beams,
resulting in the suppression of the output green and violet
beams, respectively. They also illustrate (1) for a lossless
DI to take place between two frequencies, the power must
be entirely converted to a third frequency, and (2) the
output beams of such a device depend on the phases of
all incident coherent beams. For further clarification of
the role of the relative phases, we also show in Figs. 1(d)
and 1(f) the two-wave analogues of the destructive inter-
ference scenarios shown in Figs. 1(c) and 1(e).

Akin to the conceptual three-wave converter depicted in
Fig. 1, the JPC is a nondegenerate device with spatial and
temporal separation between the idler and signal modes. Its
input and output fields share, however, the same spatial
port as shown in Fig. 2(a) and must therefore be separated
using a circulator. The idler and signal modes of the JPC
are differential modes of the microstrip resonators of the
device which intersect at a Josephson ring modulator
(JRM) [17], as shown in Fig. 2(b). The third mode sup-
ported by the device is a nonresonant common-mode drive
(pump), whose frequency f_P is set to either the sum of the
idler f_I and signal f_S frequencies or their difference. In the
case where the pump frequency satisfies $f_P = f_I + f_S$,
the device serves as a quantum-limited amplifier which
can be used to read out the state of a solid state qubit in
real-time [19,20]. In the present case where the pump
frequency verifies $f_P = f_I - f_S$ ($f_I > f_S$), the device
operates in frequency conversion mode with no photon
gain. In this mode, as opposed to amplification [16], the
device is not required, according to Caves' theorem [21], to
add any noise. Note that this working regime has been
recently the subject of several works in the areas of tele-
communication and quantum information processing in
optics [4–6,22–24]. Also, in the recent work done at
NIST [8,9], the authors parametrically converted photons
of different frequencies inside a microwave resonator
coupled to a dc-SQUID. Phonon-photon parametric
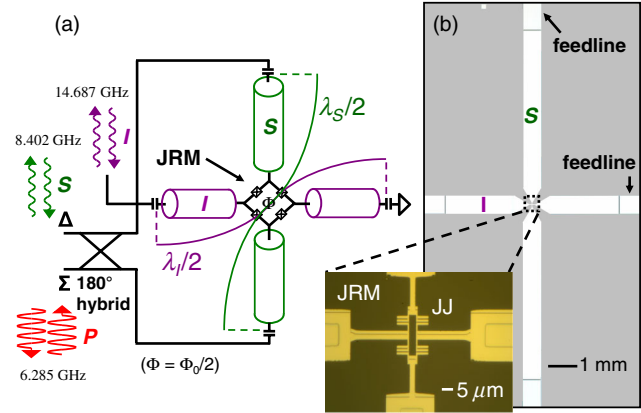frequency conversion is also at play in the active cooling

FIG. 2 (color online).   Panel (a): circuit diagram of the JPC
device. The JPC consists of two half-wave microstrip resonators
denoted (S) and (I) which resonate at $f_S = 8.402$ GHz and $f_I =
14.687$ GHz with bandwidths of 95 MHz and 270 MHz, respec-
tively. The two resonators intersect at a JRM, which consists of
four nominally identical Josephson junctions. The JRM is biased
near half a flux quantum. Both S and I modes are excited
differentially, while the pump (P) mode is commonly driven.
Thus, S and P share the same spatial input ports and are fed
through the difference (Δ) and sum (Σ) ports of a 180 degree
hybrid. Panel (b): false color optical micrographs of the JPC
device and the JRM.

of a micromechanical or nanomechanical resonator
mode [1,25,26]. In our work, by contrast, it is photons
from two different spatial and temporal modes that are
interconverted.

When operated in conversion mode and under the stiff
pump condition, the JPC can be described as an effective
two-port beam splitter whose scattering parameters can be
adjusted by varying the pump tone of the device. In this
mode, part of the incoming wave at the idler (signal) port is
transmitted to the signal (idler) port after being down-
converted (up-converted) via emission (absorption) of
pump photons, while the remaining part is reflected off
the idler (signal) port.

In Fig. 3(a) we display measurements of the reflection
parameter $|r|^2$ at the signal port (filled red circles) and the
idler-to-signal conversion parameter $|t'|^2$ (filled blue
circles) as a function of the normalized applied pump power
P_P/P_{P0}, where P_{P0} is the pump power at which $|r|^2$ is
minimum. In the reflection measurement, a coherent tone
at $f_S = 8.402$ GHz is applied to the signal port with input
power $P_{S0} = -123$ dBm, which corresponds to about 0.1
photons on average in the signal resonator, while in the
conversion measurement an equivalent coherent tone at
$f_I = 14.687$ GHz is applied to the idler port [as shown in
Fig. 3(c)]. The frequency of the applied pump tone is $f_P =
6.285$ GHz. Both measurements are taken using a spectrum
analyzer centered at f_S in zero frequency span mode. The
output power measured as a function of P_P/P_{P0} is normal-
ized relative to the reflected signal power obtained with no
applied pump power. There, the JPC has unity reflection,
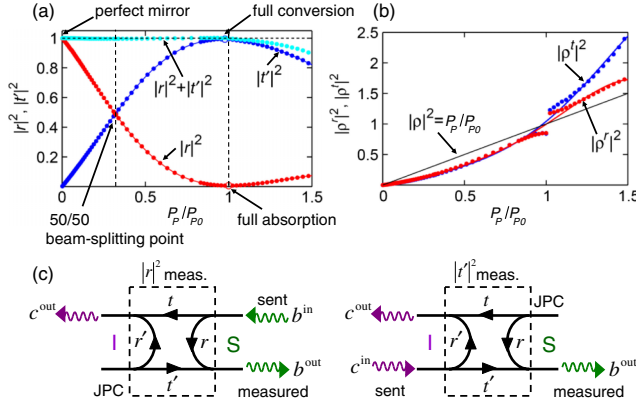
FIG. 3 (color online).   (a) Reflection and conversion measurements of the JPC. The reflection (conversion) parameter $|r|^2$ ($|t'|^2$) drawn as filled red (blue) circles, respectively, is measured at the signal port as a function of the normalized applied pump power. In the reflection (conversion) measurement, a signal (idler) tone is applied at f_S (f_I) and the pump frequency is set to $f_P = f_I - f_S$. The cyan filled circles represent the sum $|r|^2 + |t'|^2$. The red and blue lines correspond to theory expressions [27] $|t'|^2 = 4|\rho^t|^2/(1 + |\rho^t|^2)^2$ and $|r|^2 = (1 - |\rho^r|^2)^2/(1 + |\rho^r|^2)^2$. Panel (b) uses same red (blue) circles to show the relation between the dimensionless parameter $|\rho^r|^2$ ($|\rho^t|^2$) employed in the fit of the reflection (conversion) data, and P_P/P_{P0}. The black line corresponds to the relation $|\rho|^2 = P_P/P_{P0}$. The red and blue curves are polynomial fits. (c) Signal flow graphs of the JPC in the conversion mode. In the reflection and conversion measurements shown on the left and the right, equal coherent beams are applied to the signal and idler ports, respectively.

which can be measured within ± 0.5 dB accuracy due to a finite impedance mismatch in the output line.

As can be seen in Fig. 3, the splitting ratio between the converted and reflected portions of the beam is set by the device parameters and the pump amplitude. By varying the intensity of the pump, the splitting ratio of the device can be changed continuously from zero conversion and total reflection, to complete conversion and perfect absorption. It is important to mention that the input power applied to the idler port in the conversion measurement is set to yield, at the 50/50 beam-splitting working point, the same signal output power as the one measured in reflection for P_{S0}. It is remarkable that with this single calibration of input powers, which balances the output at the 50/50 beam-splitting point, the device satisfies quite well the equation of conservation of total photon number $|r|^2 + |t|^2 = 1$ ($|t| = |t'|$) in the range $P_P/P_{P0} < 1$ (see the cyan circles). When the critical power is traversed $P_P/P_{P0} \gtrsim 1$, we observe a progressive breaking of unitarity $|r|^2 + |t'|^2 < 1$. This can be explained by increased nonlinear effects at elevated pump powers resulting in frequency conversion to higher modes of the system. However, we find that in the vicinity of P_{P0}, the conversion loss defined as the deviation of $|r|^2 + |t'|^2$ from unity is less than $\pm 10^{-2}$ within $\pm 2.5\%$ accuracy. We also observe

a slight shift in power between the peak of the conversion and the minimum of the reflection data. The solid blue and red curves drawn using the equations listed in the caption of Fig. 3 correspond to theory expressions for the conversion and reflection parameters, respectively [27]. In Fig. 3(b) we use filled red and blue circles to plot the dimensionless pump power parameters $|\rho^r|^2$ and $|\rho^t|^2$, which are used to fit the reflection and conversion data as a function of P_P/P_{P0}. The solid black line satisfying the relation $|\rho|^2 = P_P/P_{P0}$ corresponds to the expected dependence of $|\rho|^2$ on P_P/P_{P0} for the ideal JPC model with stiff pump approximation. The solid red and blue curves are polynomial fits to the $|\rho^r|^2$ and $|\rho^t|^2$ parameters. The fits satisfy three important properties: (1) they pass through the origin ($|\rho^{r,t}|^2 = 0$ for $P_P = 0$); (2) they have a leading linear term in the limit of small pump powers; (3) the fits for $|\rho^r|^2$ and $|\rho^t|^2$ coincide for $P_P/P_{P0} < 1$. They therefore show that the parameter $|\rho|^2$ is in fact a renormalized pump strength, at least for $P_P/P_{P0} < 1$.

In addition to the device dependence on pump power shown in Fig. 3, the relative pump phase plays an important role as well. The down-converted idler and the up-converted signal acquire a phase shift which depends on the pump phase. We utilize this phase dependence as shown in Fig. 4 in order to sensitively interfere signal and idler beams. In this measurement, we applied two coherent tones to the signal and idler ports having the same frequencies and powers as in the measurement of Fig. 3. We have also phase-locked the three independent coherent waves to the 10 MHz reference oscillator of a rubidium atomic clock. The color mesh in Fig. 4 depicts the interference fringes of the reflected and converted signals generated at the signal port as a function of P_P/P_{P0} and the relative pump phase. As can be seen in
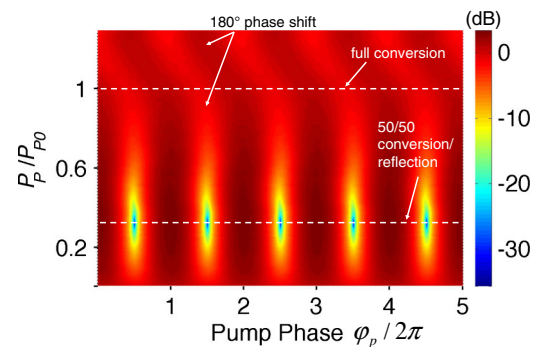

FIG. 4 (color online).   Interference fringes of the reflected signal and the converted idler measured at the output of the signal port, at f_S, as a function of pump power and phase. The top (bottom) dashed line indicates the full conversion (50/50 beam splitting) working point where the interference contrast is lowest (highest). For $P_P/P_{P0} > 1$ ($|\rho|^2 > 1$), a phase shift is observed in the interference pattern due to the change in the sign of the reflected signal amplitude, in accordance with theory [27].
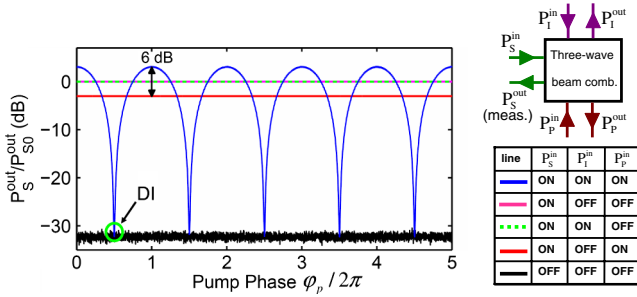
FIG. 5 (color online). The blue curve is a cross section of the interference fringes shown in Fig. 4 at the 50/50 beam-splitting working point. The maximum and minimum points of the curve correspond to constructive and destructive interference conditions, respectively. The other lines correspond to different reference measurements taken under the same experimental conditions as explained in the text. The input beams applied in each measurement are given in the table and described in the device schematics on the right.

the figure, the interference contrast is low for $P_P \ll P_{P0}$ and $P_P/P_{P0} \to 1$ which correspond to almost total reflection and conversion, respectively. A maximum interference contrast is obtained, on the other hand, for P_P/P_{P0} close to 0.32. We interpret this point as that where our device functions as a 50/50 beam splitter or combiner. This is further shown in Fig. 5, where we display a cross section of Fig. 4 at the point of maximum interference contrast. The wave interference modulation curve shown in blue is plotted as a function of the relative phase of the pump. The other lines represent different reference measurements taken under the same experimental conditions. The magenta line corresponds to the reflected signal power P_{S0}^{out} obtained without pump or idler tones and forms the reference level for the other measured powers. The dashed green line corresponds to the reflected signal power obtained with no pump but with an equivalent idler tone injected through the idler port. The fact that the dashed green line coincides with the magenta line shows that without pump the idler and signal modes are isolated. The red line represents the reflected signal power at the 50/50 beam-splitting working point and lies -3 dB below the reference (magenta) line as expected. Also, the relative power level of the peaks in the wave interference curve (blue), which correspond to constructive interference condition, lie as expected 6 dB (a factor of 4) above the red line obtained without the idler. The black line corresponds to the noise floor measured without any signal. This noise is dominated by the high electron mobility transistor (HEMT) amplifier noise connected at the 4 K stage of our setup. Note that the minimum points of the wave interference curve (blue) correspond to the DI condition and coincide with the HEMT noise floor. By calculating the ratio of the average output power received in destructive and constructive interference experiments [27], we get a lower bound of -37.9 dB on the amount of destructive interference

achieved by the device. This is equivalent to a coherent cancellation of 99.98% of the input signal and idler beams.

Furthermore, in a separate interference measurement in which we varied the input power of the signal and idler beams [27], we find that the device can handle a maximum input power of about -100 dBm, which corresponds to an average photon occupancy in the device of about 20 photons. Similar to Josephson amplifiers, this figure of merit can be improved by about 1 order of magnitude by increasing the critical current of the junctions [17,18]. We also note that the bandwidth of the present device (~ 70 MHz) is limited by the bandwidths of the resonators. A wider bandwidth (~ 500 MHz) could potentially be achieved by substituting the present JRM design with an inductively shunted ring [28].

In addition to quantum information transduction, the device has several potential useful applications, such as cooling of a readout cavity of a qubit by swapping the "hot" cavity photons, for instance, at 8 GHz, by "cold" reservoir photons at 15 GHz, and realization of a Mach-Zehnder interferometer (MZI) scheme for microwaves with real-time feedback. In the latter scheme, the device would function as an interferometric 50/50 beam combiner for incoming idler and signal waves. Assuming, for example, the information is carried by the phase of the signal in the MZI setup, while the idler serves as a reference, the information can be decoded from the incoming signal by measuring the generated interference at the signal port. Moreover, the set point of the device, which yields maximum phase sensitivity, can be maintained *in situ* by compensating the shift using the pump phase.

*baleegh.abdo@yale.edu
†Present address: LPEM-UMR8213/CNRS-ESPCI ParisTech-UPMC, 10 rue Vauquelin, 75005 Paris, France.
‡michel.devoret@yale.edu

[1] A. H. Safavi-Naeini and O. Painter, New J. Phys. **13,** 013017 (2011).
[2] C. A. Regal and K. W. Lehnert, J. Phys. Conf. Ser. **264,** 012025 (2011).
[3] J. Huang and P. Kumar, Phys. Rev. Lett. **68,** 2153 (1992).
[4] S. Zaske et al., Phys. Rev. Lett. **109,** 147404 (2012).
[5] S. Ates, I. Agha, A. Gulinatti, I. Rech, M. T. Rakher, A. Badolato, and K. Srinivasan, Phys. Rev. Lett. **109,** 147405 (2012).

P H Y S I C A L   R E V I E W   L E T T E R S

[6] M. T. Rakher, L. Ma, O. Slattery, X. Tang, and K. Srinivasan, Nat. Photonics **4**, 786 (2010).

[7] S. Ramelow, A. Fedrizzi, A. Poppe, N. K. Langford, and A. Zeilinger, Phys. Rev. A **85**, 013845 (2012).

[8] E. Zakka-Bajjani, F. Nguyen, M. Lee, L. R. Vale, R. W. Simmonds, and J. Aumentado, Nat. Phys. **7**, 599 (2011).

[9] F. Nguyen, E. Zakka-Bajjani, R. W. Simmonds, and J. Aumentado, Phys. Rev. Lett. **108**, 163602 (2012).

[10] L. G. Helt, M. Liscidini, and J. E. Sipe, J. Opt. Soc. Am. B **29**, 2199 (2012).

[11] J. Tucker and D. F. Walls, Ann. Phys. (N.Y.) **52**, 1 (1969).

[12] M. A. Albota and F. N. C. Wong, Opt. Lett. **29**, 1449 (2004).

[13] A. P. Vandevender and P. G. Kwiat, J. Mod. Opt. **51**, 1433 (2004).

[14] C. Langrock, E. Diamanti, R. V. Roussev, Y. Yamamoto, M. M. Fejer, and H. Takesue, Opt. Lett. **30**, 1725 (2005).

[15] J. S. Pelc, Q. Zhang, C. R. Phillips, L. Yu, Y. Yamamoto, and M. M. Fejer, Opt. Lett. **37**, 476 (2012).

[16] N. Bergeal, F. Schackert, M. Metcalfe, R. Vijay, V. E. Manucharyan, L. Frunzio, D. E. Prober, R. J. Schoelkopf, S. M. Girvin, and M. H. Devoret, Nature (London) **465**, 64 (2010).

[17] B. Abdo, F. Schackert, M. Hatridge, C. Rigetti, and M. Devoret, Appl. Phys. Lett. **99**, 162506 (2011).

[18] B. Abdo, A. Kamal, and M. H. Devoret, Phys. Rev. B **87**, 014508 (2013).

[19] R. Vijay, D. H. Slichter, and I. Siddiqi, Phys. Rev. Lett. **106**, 110502 (2011). In this work, the authors used a degenerate, rather than nondegenerate amplifier like the JPC described in the present article.

[20] M. Hatridge *et al.*, Science **339**, 178 (2013).

[21] C. M. Caves, Phys. Rev. D **26**, 1817 (1982).

[22] S. Tanzilli, W. Tittel, M. Halder, O. Alibart, P. Baldi, N. Gisin, and H. Zbinden, Nature (London) **437**, 116 (2005).

[23] M. G. Raymer, S. J. van Enk, C. J. McKinstrie, and H. J. McGuinness, Opt. Commun. **283**, 747 (2010).

[24] N. K. Langford, S. Ramelow, R. Prevedel, W. J. Munro, G. J. Milburn, and A. Zeilinger, Nature (London) **478**, 360 (2011).

[25] J. D. Teufel, T. Donner, D. Li, J. W. Harlow, M. S. Allman, K. Cicak, A. J. Sirois, J. D. Whittaker, K. W. Lehnert, and R. W. Simmonds, Nature (London) **475**, 359 (2011).

[26] R. Rivière, S. Déléglise, S. Weis, E. Gavartin, O. Arcizet, A. Schliesser, and T. J. Kippenberg, Phys. Rev. A **83**, 063835 (2011).

[27] See Supplemental Material at http://link.aps.org/supplemental/10.1103/PhysRevLett.110.173902 for calculation of the scattering matrix of the JPC in the conversion mode, additional interference measurements, comparison with microwave mixers, device fabrication, and measurement details.

[28] N. Roch, E. Flurin, F. Nguyen, P. Morfin, P. Campagne-Ibarcq, M. H. Devoret, and B. Huard, Phys. Rev. Lett. **108**, 147701 (2012).